ChemSusChem

Research Article
doi.org/10.1002/cssc.202400626

Chemistry Europe
European Chemical Societies Publishing

www.chemsuschem.org

Radical Polymer-based Positive Electrodes for Dual-Ion Batteries: Enhancing Performance with γ-Butyrolactone-based Electrolytes

Katharina Rudolf,[a] Linus Voigt,[a] Simon Muench,[b, c] Lars Frankenstein,[a] Justin Landsmann,[a] Ulrich S. Schubert,[b, c] Martin Winter,[a, d] Tobias Placke,[a] and Johannes Kasnatscheew*[a]

Dual-ion batteries (DIBs) represent a promising alternative for lithium ion batteries (LIBs) for various niche applications. DIBs with polymer-based active materials, here poly(2,2,6,6-tetramethylpiperidinyl-*N*-oxyl methacrylate) (PTMA), are of particular interest for high power applications, though they require appropriate electrolyte formulations. As the anion mobility plays a crucial role in transport kinetics, Li salts are varied using the well-dissociating solvent γ-butyrolactone (GBL). Lithium difluoro(oxalate)borate (LiDFOB) and lithium bis(oxalate)borate (LiBOB) improve cycle life in PTMA||Li metal cells compared to other Li salts and a $LiPF_6$- and carbonate-based reference electrolyte, even at specific currents of 1.0 $A g^{-1}$ (≈10C), whereas LiDFOB reveals a superior rate performance, *i.e.*, ≈90% capacity even at 5.0 $A g^{-1}$ (≈50C). This is attributed to faster charge-transfer/mass transport, enhanced pseudo-capacitive contributions during the de-/insertion of the anions into the PTMA electrode and to lower overpotentials at the Li metal electrode.

Introduction

The world's energy demand is steadily increasing and, thereby, the need for suitable energy storage technologies. In this context, lithium ion batteries (LIBs) dominate the battery market in various fields, *e.g.*, electro mobility, stationary storage and portable electronic devices, due to their high energy density and high specific energy.[1–3] However, the interest of other low cost, more sustainable and less toxic battery systems has grown in the past years. In particular, the most commonly used and less abundant elements in LIBs, Co and Ni, are critical for reasons of costs, low environmental-friendliness and mining conditions.[2–4]

An approach to circumvent these challenging materials is either based on materials like $LiFePO_4$ or on alternative battery technologies such as lithium-sulfur batteries or dual-ion batteries (DIBs), which make use of materials with the ability to store anions from the electrolyte at the charged state of the battery cell.[3,5–7,8] Potential materials for the positive electrode in DIBs can be *e.g.*, graphitic carbons, metal-organic frameworks or redox-active polymers.[3,5,7,9,10] Polymer-based active materials are of particular interest as, among others, the cell voltages can be tailored *via* adjusting the redox properties.[5] In comparison to *e.g.*, intercalation-based electrode materials such as graphite, polymers can frequently realize higher rate performance and long cycle life due to their simpler *i.e.*, less complex and less resistive insertion mechanism (Figure 1). Conjugated polymers often exhibit a lower reversibility and a sloping potential profile due to successive and irreversible oxidation of the polymer chain during charge. In contrast, polymers, which are connected *via* an electrochemically inactive backbone, show enhanced reversibility and distinct redox potentials and, therefore, are more reasonable for battery applications.[5,11]

Poly(2,2,6,6-tetramethyl-4-piperidinyl-*N*-oxyl methacrylate) (PTMA), which is based on the (2,2,6,6-tetramethylpiperidin-1-yl)oxyl (TEMPO) radical, has been presented first by Nakahara *et al.* in 2002 and gained interest in the field of organic batteries, because of its stable radical functional group and fast charge/discharge kinetics (*cf.* Figure 1).[5,12] Obviously, the exchange reaction between the redox centers is rather influenced by the mobility of the anion than the cation in the electrolyte,[13] which suggests a high impact of the electrolyte on the cell performance; in particular when electrodes are developed towards practical application, which includes higher active material content, higher mass loading, thus increased electrode thickness.[5,14,15] Due to TEMPO's bipolar motif, PTMA can also be used as active material for the negative electrode accompanied by cation insertion and the formation of an aminoxyl anion.

[a] K. Rudolf, L. Voigt, L. Frankenstein, J. Landsmann, M. Winter, T. Placke, J. Kasnatscheew
University of Münster, MEET Battery Research Center, Institute of Physical Chemistry, Corrensstraße 46, 48149 Münster, Germany
E-mail: johannes.kasnatscheew@uni-muenster.de

[b] S. Muench, U. S. Schubert
Laboratory of Organic and Macromolecular Chemistry (IOMC), Friedrich Schiller University Jena, Humboldtstr. 10, 07743 Jena, Germany

[c] S. Muench, U. S. Schubert
Center for Energy and Environmental Chemistry Jena (CEEC Jena), Friedrich Schiller University Jena, Philosophenweg 7a, 07743 Jena, Germany

[d] M. Winter
Helmholtz-Institut Münster, IEK-12, Forschungszentrum Jülich GmbH, Corrensstraße 46, 48149 Münster, Germany

Supporting information for this article is available on the WWW under https://doi.org/10.1002/cssc.202400626

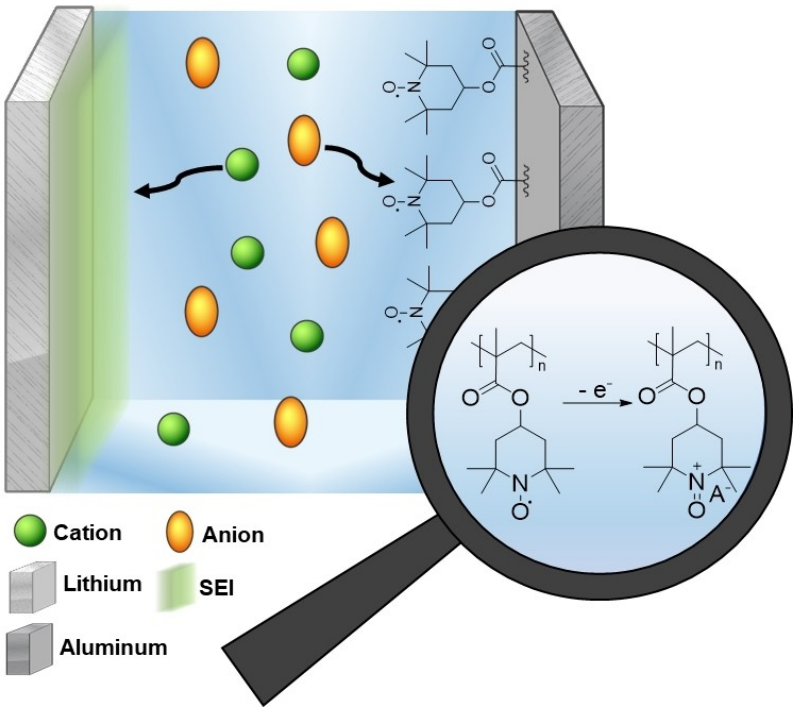

Figure 1. Schematic illustration of a PTMA-based DIB and redox reaction of PTMA.

This n-type reaction however, is not as reversible as the p-type reaction.[16]

Given the poor electronic conductivity of PTMA, high amounts of conductive carbon ($\geq$ 30 wt%) are essential for the electrode composite, however limiting its practical gravimetric/volumetric energy.[10,17] If stated, mass loadings not higher than 0.66 to 1.1 mg cm^{-2} are typical for PTMA-based electrodes in the recent literature reports, while active mass loading and total mass loading are rarely distinguished.[5,10,18,19,20] One attempt to increase the mass loading to more practical values was recently reported by Innocenti *et al.* for PTMA electrodes with a high mass loading (up to 9.65 mg cm^{-2}) along with discussing the challenges regarding commercialisation of PTMA-based batteries.[15] Enhanced electrode thicknesses have been shown to diminish the specific capacity and to increase the impedance of PTMA||Li metal cells.[14,15] Furthermore, the electrode thickness has an impact on the working mechanism of PTMA electrodes. Suga *et al.* reported a switch from a surface-controlled reaction to a diffusion-limited behaviour for the TEMPO- and polynorbornene-based positive electrode when a threshold electrode thickness (260 nm) was exceeded, and is speculated to affect the rate capability.[21] Still, solutions to surpass the challenges caused by enhanced electrode thicknesses and higher active material contents need to be found.

Carbonate-based electrolytes, state-of-the-art in LIB cells, *e.g.*, 1 M solutions of $LiPF_6$ in diethyl carbonate (DEC), dimethyl carbonate (DMC) or ethyl methyl carbonate (EMC) combined with ethylene carbonate (EC), have been evaluated initially.[5,22–24] In the meantime, also different electrolyte components and formulations have been studied in literature, like $LiClO_4$, $LiCF_3SO_3$, $LiBF_4$, and also quaternary ammonium salts in *e.g.*, propylene carbonate (PC), acetonitrile or dichloromethane.[10,25,26] $LiBF_4$ in PC, for example, revealed an enhanced mobility compared to $LiClO_4$ and $LiCF_3SO_3$,[26] which could be beneficial for rate capability and mobility in PTMA electrodes with higher thicknesses. However, often only thin PTMA coatings or electrodes with PTMA contents $<$60% were used and the impact of these electrolytes on electrodes with higher PTMA contents or higher mass loadings remains unclear.[22,23,25,26] The influence of the conducting salt was also shown for PTMA electrodes with an active mass loading of $>$8 mg cm^{-2} by comparing $LiPF_6$ with lithium bis(fluorosulfonyl)imide (LiFSI) in EC:DMC (1:1), where LiFSI led to better rate and cycling performance. However, these findings were not discussed further.[15] Moreover, ionic liquids, like 1-butyl-1-methylpyrrolidinium bis(trifluoromethanesulfonyl)imide ($Pyr_{14}TFSI$) (pure or diluted with PC) have also been studied for electrodes with a PTMA content of 60% and a mass loading in a range of 0.66 to 1.0 mg cm^{-2} with promising results, like an improved cycling performance and lower self-discharge in contrast to carbonate-based electrolytes.[10,19,20] Unfortunately, ionic liquid-based electrolytes are generally more expensive than *e.g.*, carbonate-based electrolytes, hence, alternatives need to be considered.[27]

γ-Butyrolactone (GBL), a literature-known electrolyte solvent for LIBs,[24,28,29] reveals beneficial properties, like a relatively low melting point, high boiling temperature, low viscosity, high dielectric constant and low vapour pressure. Furthermore, a major advantage is the good solubility of many Li salts in GBL, which enables application of many alternatives, which are *e.g.*, more sustainable, thermally stable or less toxic, such as, lithium bis(oxalate)borate (LiBOB), which owns a limited solubility in

carbonate-based solvents, alongside with lithium difluoro(oxalate)borate (LiDFOB) and $LiBF_4$.[24,28,30] LiBOB and LiDFOB are also known to improve the formation of an effective solid electrolyte interphase (SEI) on Li metal surfaces.[31] Additionally, $LiBF_4$ shows enhanced performance in combination with GBL in contrast to a $LiPF_6$- and GBL-based electrolyte in *e.g.*, carbon||Li metal cells.[24,32] As smaller sized ions increase the ion mobility in GBL (in case of BF_4^-, PF_6^- and $TFSI^-$),[33] this could also have an impact on the cycling performance, especially at higher rates. As the electrolyte salt is considered an active material in the DIB, a smaller and lighter anion also has a positive impact on the total energy density/specific energy.[3,34]

In this work, the impact of enhanced mass loadings on the performance is investigated for varied Li salts in GBL-based electrolytes in PTMA||Li metal cells based on electrodes with a PTMA content of 60% and an active mass loading of 1.0 mg cm^{-2} (schematic drawing *cf.* Figure 1). $LiBF_4$, $LiPF_6$, LiDFOB, LiBOB and lithium bis(trifluoromethanesulfonyl)imide (LiTFSI), with respective increase in anion size, are analysed and the impact of anion size and chemistry on the performance are systematically investigated.[33,35]

Results and Discussion

Given the impact of the Li salt on the performance of PTMA-based electrodes, the effect of the anions was systematically investigated in the solvent GBL, which is able to dissolve and dissociate a various number of Li salts.[36] Justified by preliminary cyclic voltammetry (CV) measurements of PTMA electrodes with a lower active mass loading of 0.4 mg cm^{-2} (*cf.* Figure S1) a reference $LiPF_6$/carbonate-based electrolyte was chosen. EMC-based electrolytes revealed the most promising behaviour regarding kinetic aspects (peak separation) and stability. However, linear carbonates as single solvent, especially DEC, are reactive towards Li metal, rendering them impractical with Li metal, *e.g.*, as counter electrode (CE), reference electrode (RE) or negative electrode.[37] Because of that and the similar, but slightly lower cycling performance (*cf.* Figure S2) of 1 M $LiPF_6$ in EC:EMC (1:1 by weight), $LiPF_6$ in EC:EMC (3:7 by weight; = REF) was selected as reference electrolyte, which is also commonly used in LIBs.[38] Table 1 displays all ionic conductivities of the selected electrolytes at 20 °C, where the LiDFOB-based electrolyte shows the highest ionic conductivity and the $LiBF_4$-based one the lowest.

Reversibility of Redox Reactions of PTMA

PTMA-based electrodes are known for their highly reversible redox reactions.[23] The electrode and electrolyte formulation can have a relevant impact, *e.g.*, shifting or broadening of the redox peaks due to a thicker electrode coating or a higher PTMA content.[14,17] Figure 2 shows the CV data of PTMA||Li metal cells for varied electrolytes. Compared to REF, a shift of the redox peak towards higher potentials can be observed for the GBL-based electrolytes, *e.g.*, from 3.60 V to ≈3.73 V *vs.* Li|Li^+ for the oxidation peak. With increased anion size, the peaks broaden ($BF_4^- < PF_6^- <$ $DFOB^- <$ $BOB^- < TFSI^-$) and peak currents for the oxidation and reduction processes decrease, both suggesting improved kinetics for the electrolytes with smaller anions.[39] These findings, however, do not follow the trend of the ionic conductivities (Table 1) and suggest higher relevance of other factors, for example the impact of the anion on the charge-transfer in the PTMA electrode. The $LiPF_6$-based electrolytes behave differently. The peaks are slightly decreasing with ongoing cycle number and a separation of the reduction peak is visible, in particular for REF.

This behaviour cannot be observed for PTMA electrodes with lower mass loadings of ≈0.4 mg cm^{-2} (*cf.* Figure S1) and may be explained by inhomogeneities inside the electrode, which become more visible for the more sluggish kinetics of PF_6^- de-insertion. For 1 M $LiPF_6$, 1 M LiDFOB and 1 M LiTFSI in GBL small oxidation peaks are located before the main oxidation peak at ≈3.52 V *vs.* Li|Li^+, which could indicate initial decomposition reactions of the different Li salts at the electrode surface.

Impact of the Electrolyte Composition on the Rate Capability and on the Li Plating/Stripping Behaviour

Polymer-based batteries are known for high power capabilities.[5] The theoretical specific capacity of non-cross-linked PTMA is 111 mAh g^{-1}.[12] PTMA electrodes with 60% active material content in PTMA||Li metal cells could obtain specific discharge capacities between 80 and 100 mAh g^{-1} with ionic liquid-based electrolytes at 1C and decrease by 60% at 50C.[10,20] In contrast, carbonate-based electrolytes could only obtain discharge capacities of 79 mAh g^{-1} at 1C and only 8 mAh g^{-1} at 50C.[17] Also, a modified electrode design (electrospun PTMA fibers) was shown to improve the performance at 50C (109 mAh g^{-1} after 10 cycles).[40]

Figure 3a displays the rate performance of PTMA||Li metal cells for the different electrolytes. Only minor differences in the first cycle specific discharge capacities are present at the lowest specific current of 0.02 A g^{-1}, ranging from 96 to 105 mAh g^{-1} for the LiTFSI- and the LiDFOB-based electrolyte respectively.

Table 1. Ionic conductivities of the investigated electrolytes at 20 °C.

REF	1 M $LiBF_4$ in GBL	1 M $LiPF_6$ in GBL	1 M LiDFOB in GBL	1 M LiBOB in GBL	1 M LiTFSI in GBL
7.9 mS cm^{-1}	6.0 mS cm^{-1}	8.9 mS cm^{-1}	9.1 mS cm^{-1}	6.4 mS cm^{-1}	7.6 mS cm^{-1}

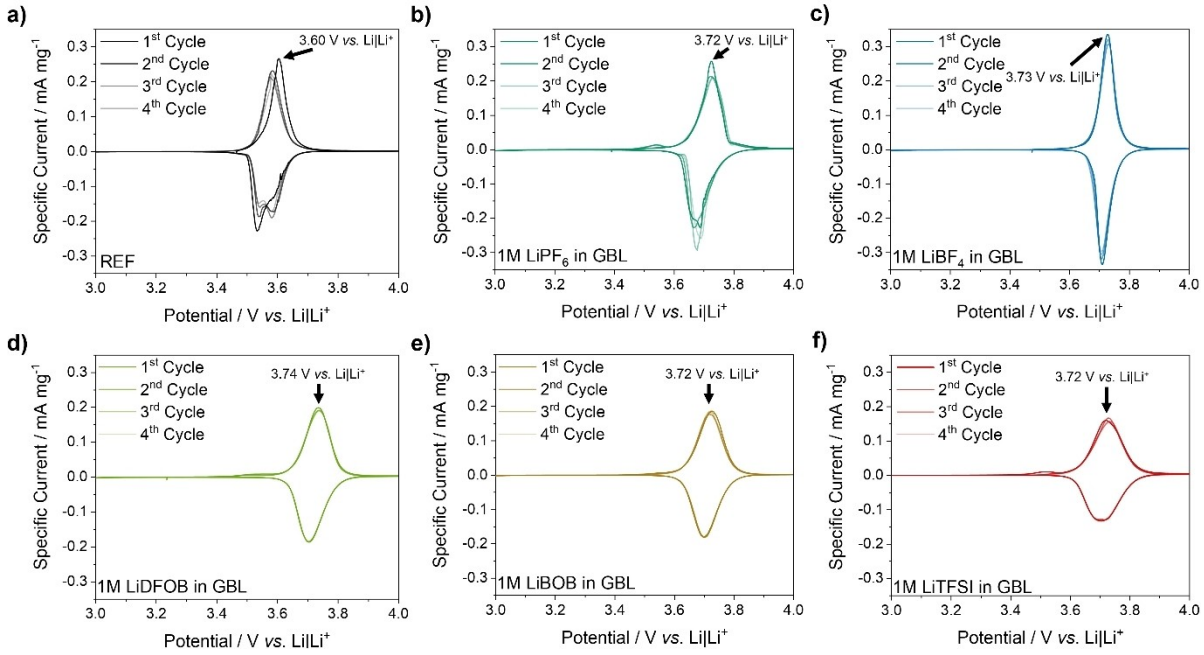

Figure 2. Specific current *vs.* potential plots of PTMA||Li metal cells (three-electrode setup) at a scan rate of 0.05 mV s^{-1} for varied electrolytes. a) REF, b) 1 M $LiPF_6$ in GBL, c) 1 M $LiBF_4$ in GBL, d) 1 M LiDFOB in GBL, e) 1 M LiBOB in GBL, f) 1 M LiTFSI in GBL.

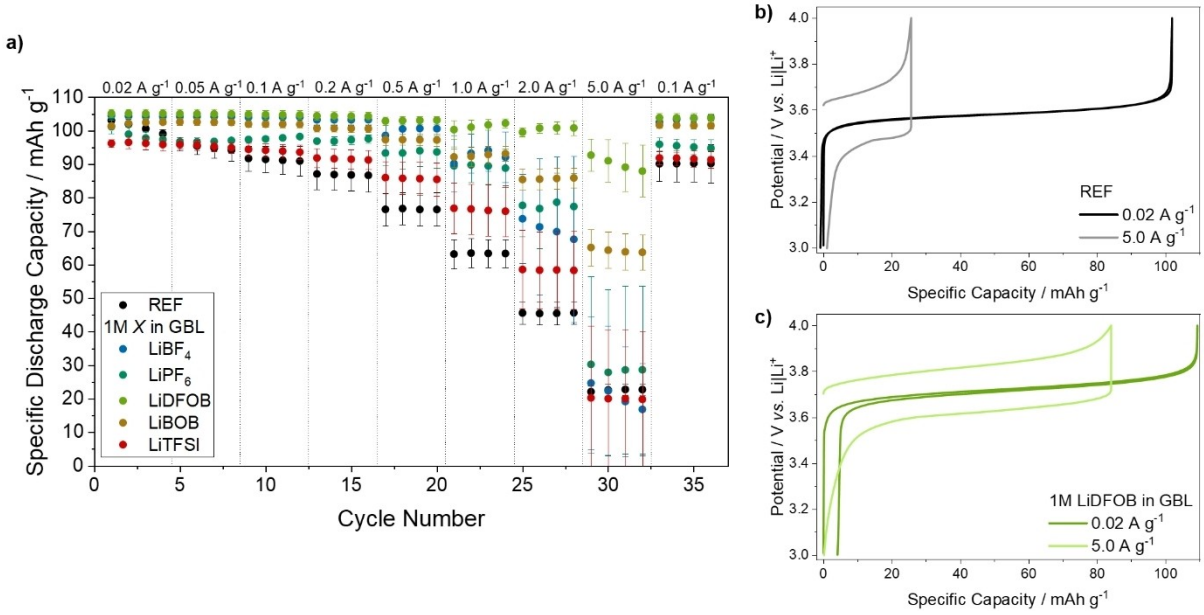

Figure 3. a) Specific discharge capacity *vs.* cycle number of PTMA||Li metal three-electrode cells for specific currents from 0.02 to 5.0 A g^{-1} and various electrolytes. Potential *vs.* specific capacity plots for the second cycle at specific currents of 0.02 and 5.0 A g^{-1} for b) REF and c) 1 M LiDFOB in GBL.

The lower capacity for the LiTFSI-based electrolyte may also originate from Al dissolution of the current collector.[41,42] The $LiPF_6$-based electrolytes reveal the highest capacity fading within the initial four cycles, which could hint at irreversible side reactions between *e.g.*, $LiPF_6$ with GBL and/or the PTMA electrode surface. Between 0.1 and 2.0 A g^{-1} all GBL-based electrolytes show improved performance compared to REF. Noticeably, the LiDFOB-based electrolyte has the smallest decay in capacity, even for a specific current of 2.0 A g^{-1}, and demonstrates a specific capacity of 100 mAh g^{-1}, compared to 46 mAh g^{-1} for REF. At a specific current of 5.0 A g^{-1} a specific capacity of 93 mAh g^{-1} can be reached (22 mAh g^{-1} for REF). Also, the LiBOB-based electrolyte shows an improved performance for higher specific currents of 85 mAh g^{-1} at 2.0 A g^{-1} and 65 mAh g^{-1} at 5.0 A g^{-1}. All cells can recover their initial specific capacities (at 0.1 A g^{-1}) after the cycling at higher rates. The potential *vs.* capacity plots of the REF and the LiDFOB-based electrolyte, seen in Figure 3b and **3c**, show no obvious

overpotentials for 0.02 A g^{-1}. Only a slight capacity loss can be seen for the LiDFOB-based electrolyte, likely related to side reactions, which is hinted by oxidation peak in Figure 2d. For a specific current of 5.0 A g^{-1}, higher overpotentials and a lower specific capacity can be seen for REF, which can be attributed to kinetic limitations of the carbonate-based electrolyte in the PTMA electrode.

Some of the investigated Li salts (*e.g.*, LiDFOB, LiBOB) are literature-known to be beneficial for Li metal negative electrodes because of *e.g.*, the improved Li plating/stripping behaviour.[43,44] Here, the suitability with GBL is evaluated in symmetric Li metal||Li metal cells (Figure 4). Similar low overvoltages for low current densities (between 0.023 and 0.035 V at 0.1 mA cm^{-2}) can be seen, while the $LiPF_6$-based electrolytes show overvoltages ranging from 0.11 to 0.24 V. For 1 M $LiPF_6$ in GBL, a notable growth in overvoltage can be seen (up to 0.48 V for 0.5 mA cm^{-2}), while LiDFOB- and LiBOB-based electrolytes exhibit the lowest overvoltages ($\approx$0.11 V). For current densities $>$1.0 mA cm^{-2} "voltage noise" can be seen for 1 M $LiPF_6$ in GBL, which in literature is frequently attributed to short-circuits caused by Li metal dendrites; being literature-known and observed/validated not only in Li cells but also in LIBs at abusing conditions (*e.g.*, high voltage).[45,46] At current densities of 2.5 mA cm^{-2} all electrolytes show an increase in overvoltages. However, this is more pronounced for the $LiBF_4$-, LiTFSI- and LiBOB-based electrolytes (max. overvoltages: 1.09, 0.81 and 1.09 V). REF and 1 M LiDFOB in GBL exhibit the best performance for the highest current densities ($\approx$0.40 V) and seem to be the most suitable electrolytes for cycling Li metal cells at higher C-rates.

Further, rate capability investigations were conducted with an activated carbon CE to exclude any impact of the Li metal electrode (Figure S3, *cf.* supporting information). All cells with GBL-based electrolyte show superior performance in comparison to REF. 1 M LiDFOB in GBL still exhibits the best performance demonstrating a beneficial influence of the GBL-based electrolytes not only on the Li metal electrode, but also on the PTMA electrode.

Long-term Cycling of PTMA||Li Metal Cells

Figure 5a displays the long-term cycling performance of PTMA||Li metal coin cells at a specific current of 0.1 A g^{-1}. All cells start with similar initial specific discharge capacities of $\approx$100 mAh g^{-1}. Both, 1 M $LiPF_6$ and 1 M LiTFSI in GBL show pronounced capacity fading. Possible reasons for this behavior can be related with slight dissolution of the Al current collector in the case of LiTFSI with ongoing cycling, leading also to a loss of the conducting salt, thus capacity.[41,42] For the $LiPF_6$-based electrolyte, other side reactions, *e.g.*, $LiPF_6$ with the aluminium oxide coating of the separator or with GBL, could take place and affect performance.[47] In both cases, the Coulombic efficiency (C_{Eff}) is lower compared to the other electrolytes

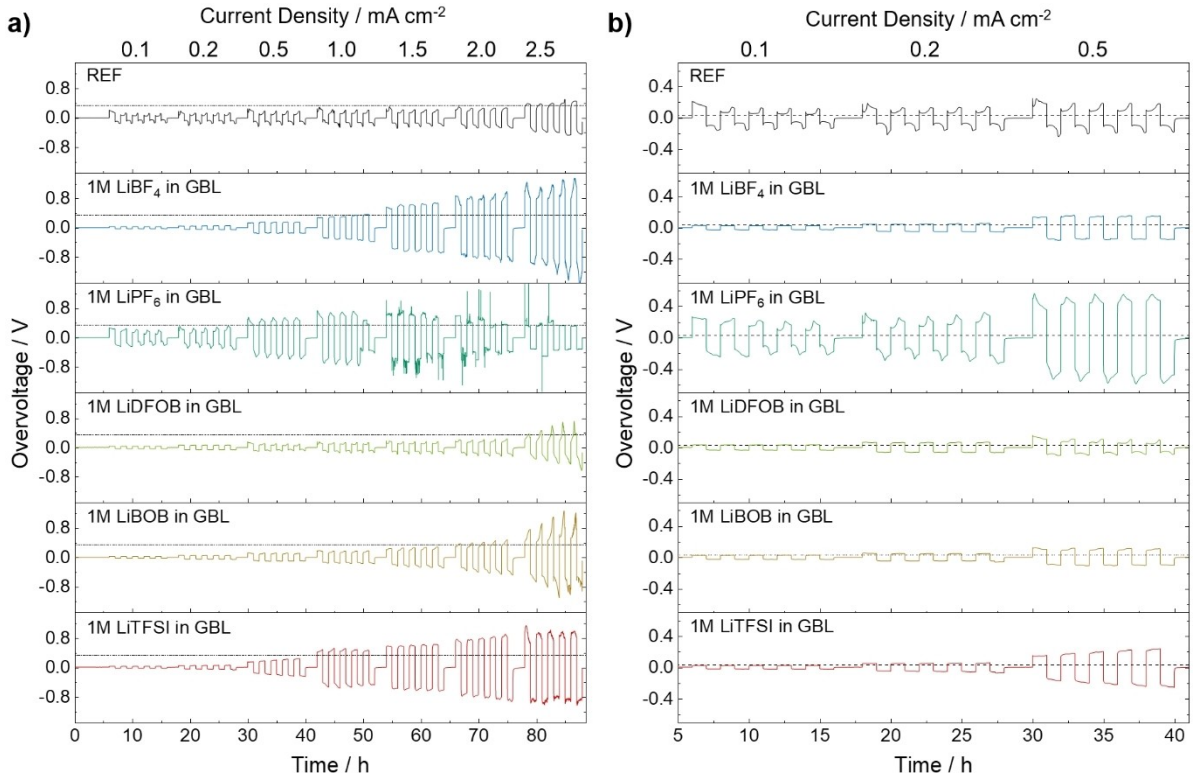

Figure 4. Overvoltage *vs.* time for Li metal||Li metal coin cells at current densities of 0.1, 0.2, 0.5, 1.0, 1.5, 2.0 and 2.5 mA cm^{-2}. a) Complete measurement, where the dotted line marks the overvoltage of the first cycle of the highest current density for 1 M LiDFOB in GBL; b) excerpt of the measurement showing the resulting overvoltages in the range of 0.1 to 0.5 mA cm^{-2}; here the dotted line marks the overvoltage of the first cycle of the lowest current density of 1 M LiDFOB in GBL.

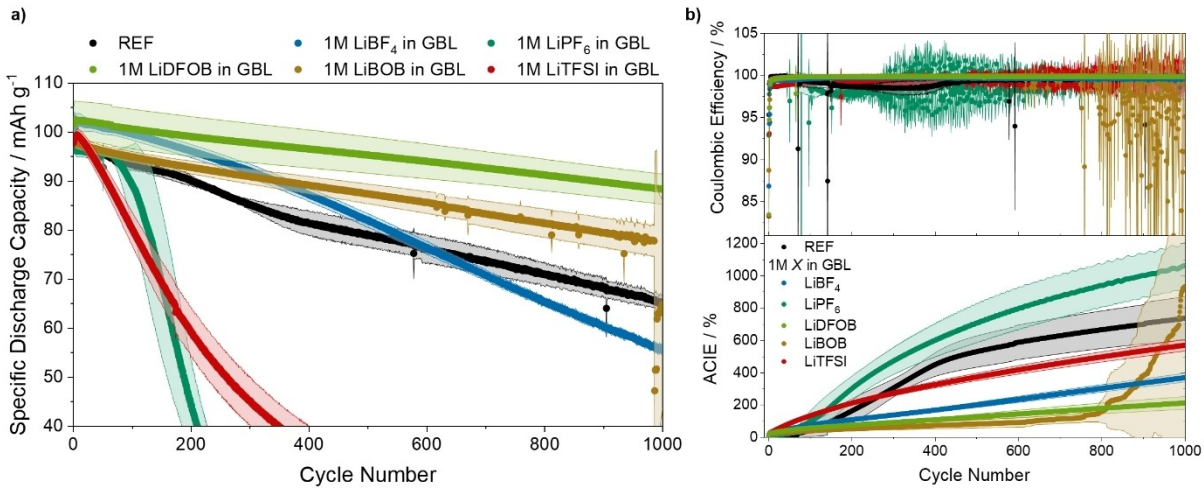

Figure 5. a) Long-term cycling of PTMA||Li metal two-electrode coin cells cycled with a specific current of 0.1 A g^{-1} and a cell voltage range of 3.0 to 4.0 V. b) C_{Eff} and ACIEs.

(Figure 5b), being an additional indication for capacity-consuming and/or impeding side reactions.

Although REF shows a relatively stable cycle life and a specific capacity of 65 mAh g^{-1} after 1000 cycles, the C_{Eff} is comparably low, in particular between the 100th and 450th cycle. This could be a result of the electrolyte reacting with the separator, inhomogeneous Li metal deposition or other side reactions of the electrolyte components.[46,47] The $LiBF_4$-based electrolyte shows high specific capacities in the beginning, however, capacity fading can be observed (56 mAh g^{-1} after 1000 cycles). The LiDFOB- and LiBOB-based electrolytes demonstrate the best cycle life. However, for the LiBOB-based electrolyte, Li dendrite formation occurs after 800 cycles, which is indicated by the fluctuation of the C_{Eff} (*cf.* Figure 5b).[48] Due to the comparably high specific capacity, more anions and Li^+ cations are inserted/plated into/onto the referring electrode in contrast to cells with a lower capacity and worse performance (*e.g.*, 1 M $LiBF_4$ in GBL). This leads to enhanced and more inhomogeneous Li deposition on the Li metal electrode and, therefore, to enhanced dendrite formation although the Li plating and stripping behavior is better compared to the $LiBF_4$-based electrolyte (*cf.* Figure 4). In the case of the LiDFOB-based electrolyte a capacity retention of 81 % was reached after 1000 cycles (88 mAh g^{-1}). This trend can also be seen in the accumulated Coulombic inefficiency (ACIE) plots (Figure 5b), where this electrolyte exhibits the lowest increase indicating reduced parasitic side reactions. The initial C_{Eff} however is one of the lowest indicating decomposition of the electrolyte. It is assumed that the LiDFOB leads to a formation of an effective SEI on the Li metal electrode, which explains the general good C_{Eff} in the following cycles.[43]

The difference between mean charge and discharge voltage (ΔV) as function of the cycle number provides indications with respect to the total cell resistance (Figure 6).[49] In line with the cycling performance, the cells containing 1 M $LiPF_6$ and 1 M LiTFSI in GBL show higher ΔV values caused by higher overvoltages. In the case of LiTFSI, ΔV is steadily increasing, which could be a hint for ongoing decomposition reactions, *e.g.*, Al dissolution,[41,42] or the formation of a thicker SEI leading to a rise in resistance on the Li metal electrode. Both $LiPF_6$-based electrolytes show a higher ΔV after the formation cycles. After decreasing up to the 150th cycle, the ΔV is increasing

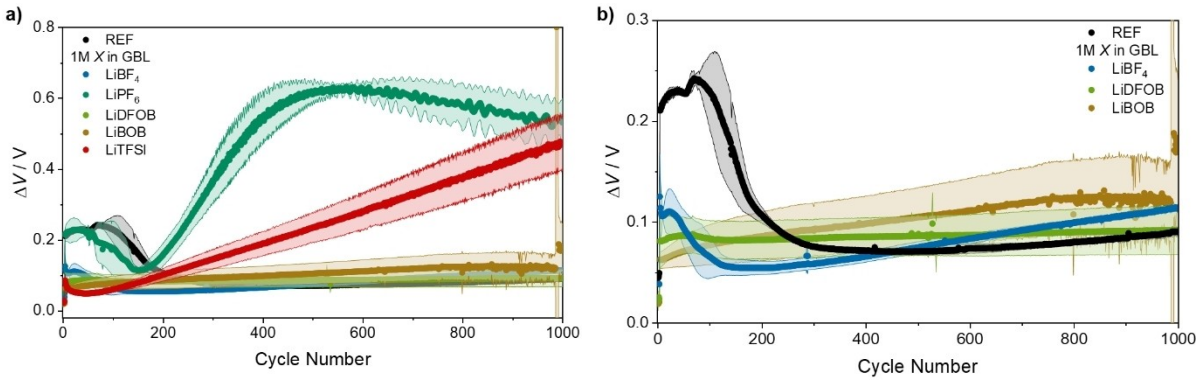

Figure 6. ΔV *vs.* cycle number of PTMA||Li metal two-electrode coin cells cycled at 0.1 A g^{-1} using different electrolytes. a) Comparison of all investigated electrolytes. b) Excerpt of the four best performing electrolytes.

again. This could be caused by the overvoltages at the Li metal electrode surface, as shown before in Figure 4. The current densities in the first cycles (0.1 mA cm^{-2}) of the Li plating and stripping experiments are comparable to the current densities in the PTMA||Li metal full cells at 0.1 A g^{-1}. There, the Li metal||Li metal cells reveal overvoltages of more than 0.08 to 0.22 V for the $LiPF_6$-based electrolytes compared to the other electrolytes. These differences in the ΔV can also be seen in Figure 6. REF shows a ΔV of 0.22 V compared to 0.08 V for 1 M LiDFOB in GBL. With ongoing cycling, more dendritic Li is forming, leading to more SEI formation, but also to a decrease in current density, because of the increasing surface area. This could be an explanation for the first increasing and afterwards decreasing ΔV. In conclusion, the main cause for the obtained ΔV values seems to be the reactions of the respective electrolytes on the Li metal surface. However, effects on the PTMA surface cannot be excluded.

The trends of the mentioned cycling experiments are more pronounced for a specific current of 1.0 A g^{-1} (Figure 7a). The $LiBF_4$- and the LiTFSI-based electrolyte show increased capacity fading and only less than 10 mAh g^{-1} after 1000 cycles. The ACIE plots (Figure 7b) support the trend of the capacity. Both electrolytes show lower C_{Eff} and thereby a faster increasing ACIE, due to more side reactions. Furthermore, the comparably low conductivity of the $LiBF_4$-electrolyte (*cf.* Table 1) could have a higher impact at higher rates, causing slower kinetics, thus lower capacities. The LiBOB-based electrolyte has the highest initial capacity (86 mAh g^{-1}), but fades to 55 mAh g^{-1} after 1000 cycles, though the fading is lower compared to the LiTFSI- or $LiBF_4$-based electrolytes. This improved cycling behaviour could be caused by the good Li plating and stripping behaviour at higher rates (Figure 4). Although, the LiDFOB-based electrolyte starts at a lower specific capacity of ≈60 mAh g^{-1}, the capacity is rising until a specific capacity of 90 mAh g^{-1} is reached after 850 cycles, which could be caused by initial overvoltages. With ongoing cycling, the PTMA might be swelling, leading to a decrease in overvoltages and more accessible PTMA in the electrode. Depending on the interactions of the used Li salt and the PTMA, the swelling of the PTMA or the overvoltages at the electrode surface can be affected. With further cycling, the capacity is decreasing again until a capacity of 81 mAh g^{-1} can be obtained after 1000 cycles. Both, the LiDFOB- and the LiBOB-based electrolyte, show also a superior ACIE in comparison to the $LiBF_4$- and LiTFSI-based ones (Figure 7b). The capacity fading of the cells using either the LiDFOB- or the LiBOB-based electrolyte may be caused by incomplete Li stripping on the Li metal negative electrode and anion trapping inside the PTMA positive electrode due to higher overpotentials present on both electrodes at these specific currents. This can also be seen in the rate capability and Li metal plating/stripping tests (Figure 3 and Figure 4).

Both $LiPF_6$-based electrolytes show a completely different behaviour. After three regular formation cycles, receiving between 96 and 99 mAh g^{-1}, the capacity drops to almost 0 mAh g^{-1} after changing the specific current to 1.0 A g^{-1}. This behavior cannot only be related to the Li metal electrode, in particular in the case of REF, which exhibits a lower overvoltage during Li plating and stripping compared to *e.g.*, 1 M LiTFSI in GBL (*cf.* Figure 4). Instead, this may be caused by the interaction of the PF_6^- anion with the PTMA electrode. The cell voltage *vs.* specific capacity plots (Figure 8) display worse kinetics of both $LiPF_6$-electrolytes compared to the other electrolytes.

The cell voltage shows the usual plateaus for the 1st cycle at a specific current of 0.02 A g^{-1} (3.72 to 3.73 V for GBL-based electrolytes, 3.61 V for REF). In contrast, the plateau of the oxidation reaction of the PTMA in the 4th cycle is shifted to higher voltages, followed by a large voltage drop after reaching 4 V, indicating higher resistances (*i.e.*, Ohmic resistances). For the $LiPF_6$-based electrolytes, the voltage plateau cannot be reached completely, so the oxidation of the PTMA and the insertion of the PF_6^- into the electrode does not occur resulting in absence of reversible storage capacity. To obtain capacity, the voltage window needs to be increased. However, this enhances the risk of decomposition reactions. By taking a look at the ΔV plots (Figure 9) it can be seen, that the $LiBF_4$- and the LiDFOB-based electrolytes already start at higher values

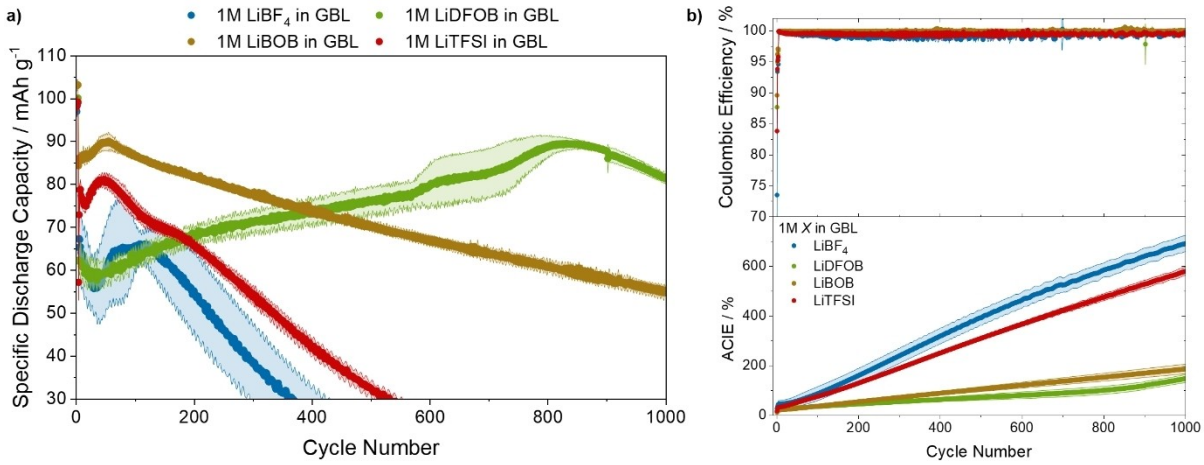

Figure 7. a) Long-term cycling of PTMA||Li metal two-electrode coin cells cycled with a specific current of 1.0 A g^{-1} and a voltage range of 3.0 to 4.0 V. b) Respective C_{Eff} and ACIE.

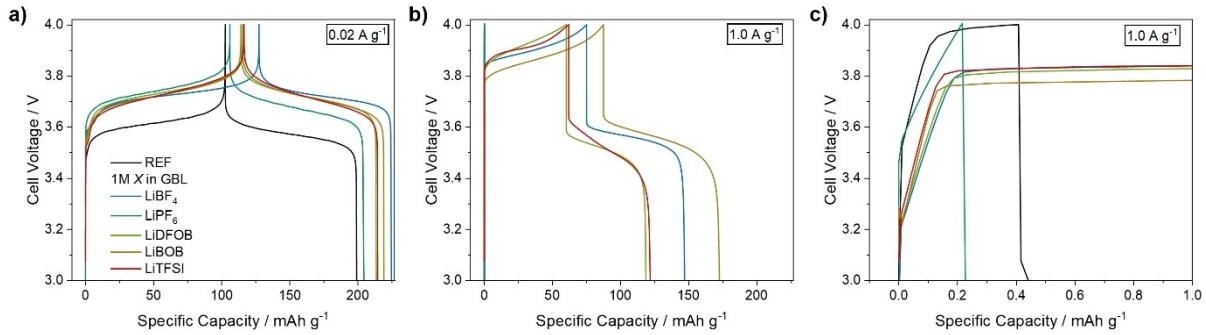

Figure 8. Cell voltage *vs.* specific capacity plots of PTMA||Li metal two-electrode coin cells of the a) 1st cycle

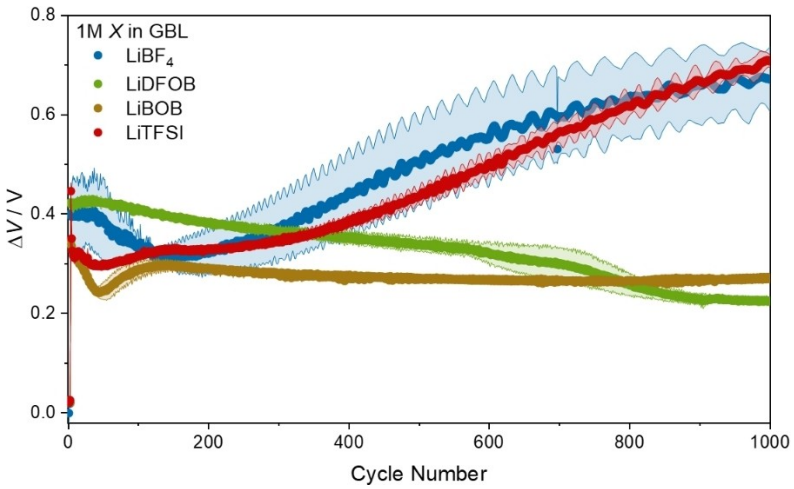

Figure 9. ΔV *vs.* cycle number of PTMA||Li metal coin cells cycled at 1.0 A g^{-1} using different electrolytes.

compared to the other two electrolytes. Nonetheless, the $LiBF_4$- and LiTFSI-based electrolytes show increasing ΔV values, confirming the trend of the specific capacities and hinting at higher resistances. The LiBOB-electrolyte shows a steady ΔV after the first 100 cycles and the LiDFOB-based one a decreasing ΔV. Both conducting salts seem to decrease the resistance, which is later validated *via* impedance measurements for the LiDFOB-based electrolyte.

Faradaic and Pseudo-Capacitive Contributions at the PTMA Electrode

To further investigate the impact of the PTMA electrode regarding the performance at higher rates, further CV measurements of PTMA||Li metal cells at different scan rates were conducted to examine the contribution of faradaic and pseudo-capacitive reactions at the PTMA electrode. Therefore, scan rates between 0.01 and 0.80 mV s^{-1} were used (*cf.* Figure 10), which correspond to ≈0.04C to 3C. Higher scan rates would lead to a shift of the oxidation peak towards potentials >4.0 V *vs.* Li|Li$^+$ for $LiPF_6$-based electrolytes.

By plotting the logarithm of the maximum specific current of each cycle *vs.* the logarithm of the scan rate and calculating the slope, the contributions of Faradaic/diffusion-limited and the pseudo-capacitive/reaction-limited processes can be estimatedfollowing the equation $i_p = av^b$ (i_p: peak current, v: scan rate), where a and b are adjustable values. A b-value of 0.5 would indicate a diffusion-limited reaction, whereby a b-value of 1.0 indicates a surface-controlled reaction.[50] Since the slope is not linear in the range of all scan rates, the graphs are divided into three regions (Figure S4). In the region of a scan rate up to 0.1 mV s^{-1} the $LiPF_6$-based electrolytes show a slightly lower slope compared to the other electrolytes (Tables 2 and 3). The highest b-value can be found for 1 M LiTFSI in GBL (0.98 for the oxidation, 1.01 for the reduction), which refers to a fully pseudo-capacitive behaviour of the PTMA-electrode in combination with this electrolyte and below a scan rate of 0.1 mV s^{-1}. Also, the cell containing 1 M $LiBF_4$ in GBL shows a b-value of 0.99 for the reduction process. In the region of 0.1 to 0.4 mV s^{-1} all b-values are decreasing. The lowest slope of 0.59 (oxidation) and 0.66 (reduction) can be seen for REF indicating an increase in the contribution of diffusion-limited reactions. 1 M LiTFSI in GBL reveals the highest b-value also at these scan rates implying the highest contribution of pseudo-capacitive reactions in comparison to the other electrolytes. However, 1 M LiDFOB in GBL exhibits the second highest b-values. By increasing the scan rates, all b-values decrease further, except for the LiDFOB-based electrolyte. The oxidation peaks display a slope of 0.86 and for the reduction a slope of 0.92, which

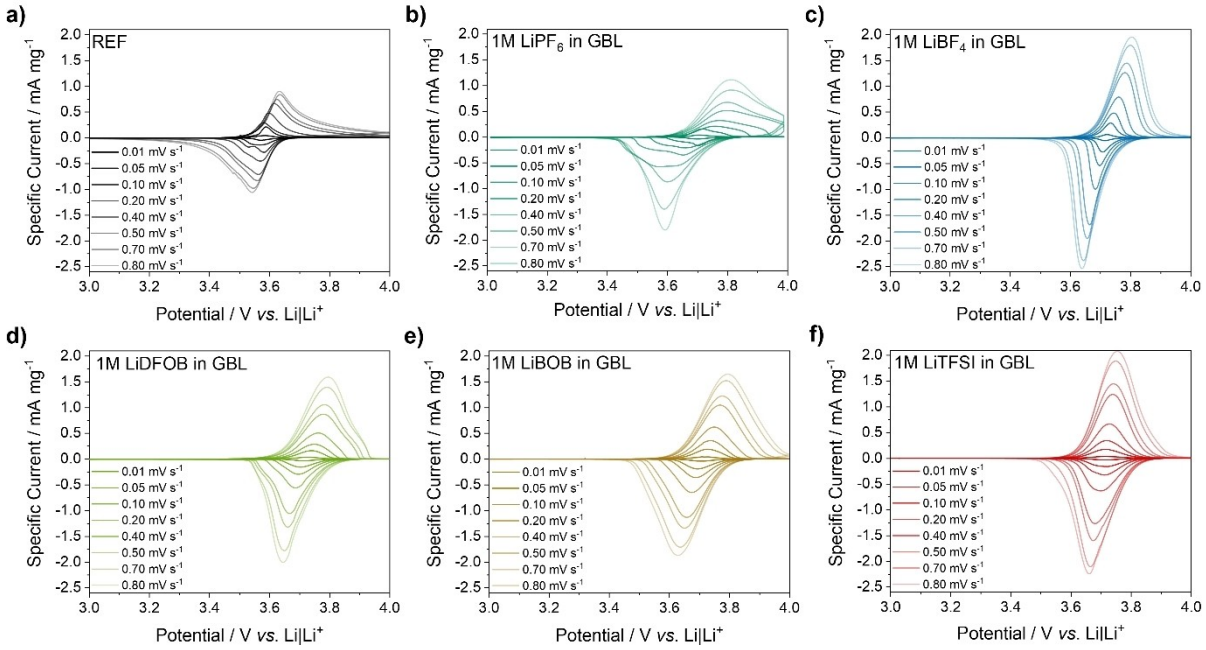

Figure 10. CV measurements of PTMA||Li metal three-electrode cells using scan rates ranging from 0.01 to 0.8 mV s^{-1}. a) REF, b) 1 M $LiPF_6$ in GBL, c) 1 M $LiBF_4$ in GBL, d) 1 M LiDFOB in GBL, e) 1 M LiBOB in GBL and f) 1 M LiTFSI in GBL.

Table 2. *b*-Values for the oxidative peak current of PTMA||Li metal cells using different electrolytes.

Electrolytes	***b*-value**		
	$\leq$0.1 mV s^{-1}	0.1 mV s^{-1} $\leq v \leq$ 0.4 mV s^{-1}	$\geq$0.4 mV s^{-1}
REF	0.85 ± 0.12	0.59 ± 0.07	0.42 ± 0.02
1 M $LiBF_4$ in GBL	0.89 ± 0.04	0.70 ± 0.01	0.63 ± 0.00
1 M $LiPF_6$ in GBL	0.75 ± 0.10	0.65 ± 0.02	1.07 ± 0.06
1 M LiDFOB in GBL	0.90 ± 0.02	0.80 ± 0.01	0.86 ± 0.02
1 M LiBOB in GBL	0.93 ± 0.01	0.78 ± 0.01	0.66 ± 0.01
1 M LiTFSI in GBL	0.98 ± 0.00	0.93 ± 0.02	0.75 ± 0.02

Table 3. *b*-Values for the reductive peak current of PTMA||Li metal cells using different electrolytes.

Electrolytes	***b*-value**		
	$\leq$0.1 mV s^{-1}	0.1 mV s^{-1} $\leq v \leq$ 0.4 mV s^{-1}	$\geq$0.4 mV s^{-1}
REF	0.75 ± 0.08	0.66 ± 0.01	0.56 ± 0.03
1 M $LiBF_4$ in GBL	0.99 ± 0.01	0.82 ± 0.04	0.59 ± 0.02
1 M $LiPF_6$ in GBL	0.78 ± 0.15	0.73 ± 0.00	1.60 ± 0.07
1 M LiDFOB in GBL	0.94 ± 0.01	0.92 ± 0.00	0.92 ± 0.02
1 M LiBOB in GBL	0.95 ± 0.01	0.83 ± 0.01	0.73 ± 0.01
1 M LiTFSI in GBL	1.01 ± 0.00	0.98 ± 0.01	0.83 ± 0.06

indicates the combination of PTMA and LiDFOB have overall a high and for scan rates above 0.4 mV s^{-1} the highest pseudo-capacitive contributions. Seemingly, the $DFOB^-$ anion has favourable properties regarding size and charge distribution to achieve a high percentage of pseudo-capacitive behaviour. Overall, larger anions may also be advantageous for more pronounced pseudo-capacitive contributions when scan rates over 0.1 mV s^{-1} are used. The cell containing 1 M $LiPF_6$ in GBL shows no clear evaluable results. A *b*-value of over 1 was calculated for the reduction peaks at scan rates over 0.4 mV s^{-1}. A possible reason for this can be side reactions interfering with the actual CV of the PTMA-electrode. This fits to the trend of the before-shown measurements, especially the lower C_{Eff} (Figure 5b). Furthermore, it can be seen that the oxidation and reduction peaks shift apart to lower/higher potentials when the scan rates are increased (Figure 10). This behavior can be seen

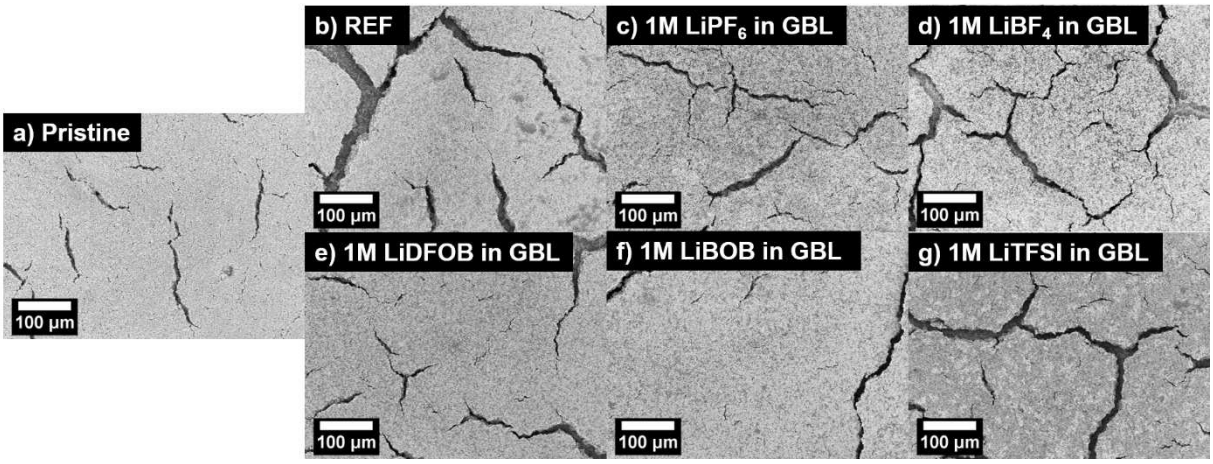

Figure 11. SEM images of PTMA electrodes after 1000 charge/discharge cycles at a specific current of 0.1 A g^{-1} (magnification 200x). a) Pristine PTMA electrode, b) REF, c) 1 M $LiPF_6$ in GBL, d) 1 M $LiBF_4$ in GBL, e) 1 M LiDFOB in GBL, f) 1 M LiBOB in GBL and g) 1 M LiTFSI in GBL.

in the voltage *vs.* specific capacity plots of the cycling at 1.0 A g^{-1} (Figure 8). The shift of the peaks can also be seen for the other electrolytes, however, not in the same extend. Although, the carbonate-based electrolyte shows a similar shift of the oxidation and reduction plateaus in the voltage plot, the peaks are not shifting as much in the CVs. It appears, that this behavior can only be seen at higher scan rates.

Surface Morphology Investigations of Cycled PTMA Electrodes

The surface of the cycled electrodes was investigated by scanning electron microscopy (SEM). Figure 11a displays the pristine PTMA electrode. Most of the electrode is covered in conductive carbon, however, smaller PTMA agglomerates ($\approx$1 µm) can be observed. Further, smaller cracks in the coating can be seen, which may be formed during the drying of the electrodes. After 1000 cycles at 0.1 A g^{-1} some differences can be observed. For all electrolytes, besides the LiDFOB- and LiBOB-based, larger cracking of the electrode can be found in comparison to the pristine electrode (Figure 11a-g). For the $LiBF_4$-based electrolyte additional decomposition products can be found on the surface (*cf.* Figure S5d). A higher tendency to decomposition at the positive electrode can also already be observed in graphite-based DIB containing $LiBF_4$-based highly concentrated electrolytes.[6] This could be an explanation for the slightly lower C_{Eff} and lower cycling performance compared to *e.g.* 1 M LiDFOB in GBL (*cf.* Figure 5). Agglomeration of PTMA ($\approx$1 to 3 µm) on the surface can be seen for all electrolytes (*cf.* Figure S5b–g). This may be the result of swelling of the PTMA by the electrolyte solvent.

Furthermore, electrodes, cycled with a specific current of 1.0 A g^{-1}, were analyzed. Since $LiPF_6$-based electrolytes prevented cell operation, no pronounced differences in comparison to the pristine electrode can be seen (Figure S6). For the $LiBF_4$- and LiTFSI-based electrolytes crack formation can be observed. Further, an increased agglomeration of the PTMA can be observed on the electrode surface, which could cause contact loss and explain capacity fading (Figure S7d and S7g). For the LiBOB- and LiDFOB-based electrolyte less cracking can be found, which correlates with the cycling performance (Figure S6e–f).

Electrochemical Impedance Spectroscopy

Electrochemical impedance spectroscopy (EIS) data of the LiDFOB- and GBL-based systems is shown in Figure 12. Measurements performed in PTMA||Li metal three-electrode cells containing a Li metal RE lead to presence of artefacts of the Li

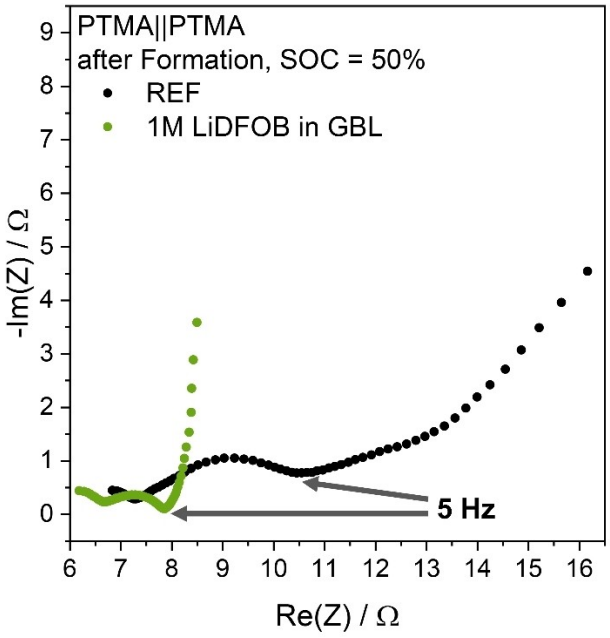

Figure 12. Nyquist plot obtained *via* EIS of PTMA||PTMA symmetric cells. PTMA electrodes were previously charged to 50 % SOC in PTMA||Li metal half-cells.

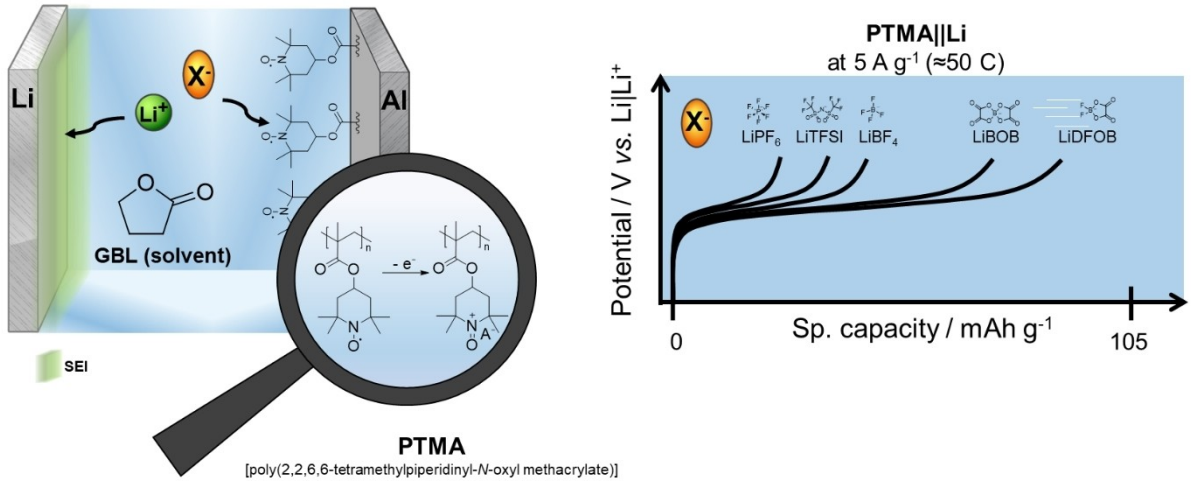

Figure 13. Schematic summary. The Li salts in GBL reveal crucial impact on the PTMA||Li metal cell performance, particularly at high rates (≈50 C).

metal CE despite the use of a RE, likely because of the much higher resistance of the Li CE in comparison to the PTMA working electrode (WE) (EIS measurements of PTMA||Li three-electrode cells *cf.* Figure S8).[51] Hence, symmetric PTMA||PTMA cells (50% state-of-charge (SOC)) are further investigated. Figure 12 depicts the resulting data of the EIS measurements. In the area of higher frequencies, a half of a semi-circle can be seen for both electrolytes. This feature can be attributed to the contact resistance of the electrodes and the other cell components.[52] This could be confirmed *via* EIS of a symmetric PTMA||PTMA cell for blocking conditions. In this case, pristine PTMA electrodes were used to remove contributions of the charge transfer resistance (*cf.* Figure S9). The area of the semi-circles of the contact resistance seems to be similar for both cases. In contrast, the second semi-circle, which can be attributed to the charge transfer or interphasial resistance, differs in size in dependency of the used electrolyte.[52] The size of the semi-circle of the cell using REF is by a multiple higher compared to the cell containing the GBL-based electrolyte. Possibly, the use of GBL and LiDFOB improves the charge transfer inside the PTMA electrode by facilitating the interaction of the PTMA, the anion and solvent molecules and/or by improved interphases. Furthermore, the charge distribution of the larger and less symmetric $DFOB^-$ anion could be favourable for the coordination of the anion to the oxoammonium cation in comparison to the harder PF_6^- anion. Generally speaking, the contribution of charge transfer resistances gets less relevant for enhanced currents in comparison to rather small currents used for *e.g.*, EIS measurements.[53] However, in this case, the overall impedance is relatively low leading to a current (during the EIS measurement), which roughly corresponds to a specific current of up to 0.5 $A g^{-1}$ (≈5C) in the frequency range, where charge transfer processes are visible. Therefore, the lower charge transfer resistances found for 1 M LiDFOB in GBL compared to REF can be one explanation for the enhanced rate performance (Figure 3a, 7a and 13).

Further, both electrolytes display different behaviour in the range of low frequencies below 5 Hz. There, the impedance contribution for restricted diffusion is higher and the phase angle appears to be smaller for REF compared to the LiDFOB-based electrolyte, which shows an almost capacitive-like behaviour.[54] This can be a hint for improved mass transport for the LiDFOB electrolyte, which may also be related to a better wetting/gelling of the PTMA.

Indication for a lower mass transport for REF can also be seen in the potential profiles at 5.0 $A g^{-1}$ (*cf.* Figure 3b and c). The potential polarises to the cut-off potential without reaching the achievable charge capacity obtained at lower specific currents. This may indicate that the critical current according to the Sand equation is exceeded by *e.g.*, slow anion diffusion in the gelled polymer.[55] Further, a faster charge transfer should mainly have an impact on the potential hysteresis, which is only slightly higher for REF compared to 1 M LiDFOB in GBL (0.22 V and 0.20 V for 5.0 $A g^{-1}$). Concluding, faster mass transport seems to play a dominant role in the enhanced rate performance related to 1 M LiDFOB in GBL.

Conclusions

In this work, different electrolyte formulations based on GBL as electrolyte solvent are investigated, where the solution of LiDFOB in GBL improves the performance of PTMA||Li metal cells compared to an LIB state-of-the-art electrolyte, *i.e.*,1 M $LiPF_6$ in EC:EMC (3:7) (REF). GBL-based electrolytes enhance the reversibility and reaction kinetics of PTMA-based electrodes, as shown in CV measurements. The rate performance of PTMA electrodes in dependence on electrolyte anions is decreasing following the order: $DFOB^- > BOB^- > BF_4^- \approx PF_6^- > TFSI^-$. Additionally, a positive effect of the GBL-based electrolytes on the Li metal negative electrode can be found for current densities of up to 0.2 $mA cm^{-2}$. The overall suitability of the different anions towards the Li metal anode is decreasing in the following order (for GBL): $DFOB^- > BOB^- > TFSI^- > BF_4^- > PF_6^-$. For current densities up to 2.0 $mA cm^{-2}$ REF and the LiDFOB- and LiBOB-based electrolytes show the best Li plating and stripping behaviour.

Charge/discharge cycling performance of PTMA||Li metal cells follow the trend of the before-mentioned experiments, especially for high specific currents (1.0 A g^{-1}), while cells containing $LiPF_6$-based electrolytes cannot even be cycled at these specific currents within the voltage range of 3.0 to 4.0 V. The improved performance of 1 M LiDFOB in GBL can be attributed to a more pseudo-capacitive capacity contributions, shown *via* CV, and a faster charge-transfer/mass transport as indicated by EIS. Furthermore, the surface of cycled PTMA electrodes after 1000 cycles reveal less cracking compared to other electrolytes, as shown *via* SEM.

The anion size seems to play a minor role and other factors, like interactions between Li salt and the electrodes are likely to be more relevant. In summary, 1 M LiDFOB in GBL is beneficial for both, the Li metal negative electrode and the PTMA positive electrode, resulting in superior performance in PTMA||Li metal cells.

The transfer of these findings on PTMA electrodes with a higher active mass loading or with other negative electrode materials requires further investigations alongside with a thorough investigation of the PTMA electrode surface, *e.g., via* X-ray photoelectron spectroscopy. Understanding of decomposition products, degradation of the electrode or passivation layers are essential to further clarify the (fading) mechanism of the investigated electrolytes.

Experimental

Electrode Preparation

PTMA-based electrodes consisted of 60 wt% cross-linked PTMA (estimated max. specific capacity 108 mAh g^{-1}; synthesis conducted and described by Muench *et al.*),[10] 30 wt% conductive carbon (C-nergy Super C65, Imerys Graphite & Carbon) and 10 wt% sodium carboxymethylcellulose (WALOCEL CRT 2000 PA, DuPont). All solid components were put in a swing mill jar (10 ml volume) containing five ZrO_2 balls (ø = 5 mm). Deionized water was added to reach a solid content of ≈12 wt%. The components were mixed in a MM400 swing mill mixer by Retsch at 15 Hz for 15 min, 20 Hz for 30 min and 30 Hz for 60 min to minimize the formation of PTMA agglomerates. Subsequently, the electrode paste was coated with a wet film thickness of 200 µm onto an aluminium foil (20 µm, SpeirA gmbH), which was cleaned with ethanol beforehand. The electrode sheets were dried at 70 °C overnight, punched out into discs with diameters of 12, 14 and 18 mm and dried at 110 °C and ≤ 10^{-3} mbar, which resulted in electrodes with an active mass loading of 1.0 mg cm^{-2} (±0.1 mg cm^{-2}).

Electrolyte Preparation

1 Molar solutions of $LiPF_6$ (Enchem, battery grade), $LiBF_4$ (BASF, 97.5 %), LiDFOB (abcr, 99 %), LiBOB (BASF, 98 %) and LiTFSI (Sigma-Aldrich, 99.95 %) in GBL (Sigma-Aldrich, battery grade) were prepared in an argon-filled glove box (O_2 and H_2O contents below 1 ppm). $LiBF_4$ and LiBOB were dried at 100 °C under reduced pressure prior to the preparation of the electrolytes. LiTFSI was first dried at 80 °C under reduced pressure for 18 h and then dried at 60 °C at 10^{-8} mbar for 24 h before use. The moisture content of LiDFOB was controlled by Karl-Fischer titration and used as received. 1 M $LiPF_6$ in EC:EMC (3:7 by wt.) (Solvionic) was used as reference electrolyte as received.

Conductivity Measurements

The ionic conductivity of each electrolyte was measured twice with an MCS 10 by BioLogic or a Zahner Zennium Pro and a TSC 1600 cell containing a glassy carbon electrode by rhd instruments. A temperature of 20 °C was used.

Cell Assembly

A three-electrode T-cell by Swagelok was utilized for CV and rate capability experiments. Thereby, the PTMA electrodes were used as WE and lithium metal (Gelon) was applied as CE (ø = 12 mm) and RE (ø = 5 mm). Three layers of a non-woven polymer separator (polypropylene, Freudenberg 2226) with a diameter of 13 mm soaked with 110 µl electrolyte were used between the WE and CE, a 10 mm separator and 50 µl were used for the RE respectively. The T-type cells were prepared in an argon-filled glovebox. A two-electrode coin cell setup was used for Li plating and stripping experiments and for constant current cycling (CCC). For the CCC, Li metal (ø = 15 mm; Albemarle) was applied as negative electrode and a PTMA electrode (ø = 14 mm) was used as positive electrode. Four layers of Mitsubishi OZ-S30 (ceramic-coated polyethylene terephthalate) with a diameter of 16 mm, soaked with 100 µl electrolyte, were used as separator. A lower number of layers led to a higher occurrence of short circuits by Li metal dendrites. For Li plating/stripping a symmetric cell containing Li metal (ø = 15 mm; Albemarle) was used as negative and positive electrode. Three layers of Freudenberg 2226 separator (ø = 16 mm) and 160 µl electrolyte were used for this setup. All coin cells were assembled in a dry room (dew point: −50 °C). PAT-Cells by EL-Cell were used for EIS measurements. PTMA electrodes (ø = 18 mm) were used as WE and Li metal (ø = 18 mm, Albemarle) was used as CE. Li metal was utilized as RE. After formation of the PTMA electrode (*cf.* Electrochemical Investigations), the cycled PTMA electrodes were used for symmetric PTMA||PTMA cells. All PAT-Cells were assembled in an argon-filled glovebox and four layers of Mitsubishi OZ-S30 soaked with 160 µl electrolyte were used as separator.

Electrochemical Investigations

CV was used to investigate the redox reactions of the PTMA electrode and the stability of the electrodes and electrolytes. After a 6 h open circuit voltage (OCV) step for wetting purposes, a potential range of 3.0 to 4.0 V *vs.* Li|Li^+ was applied with a scan rate of 0.05 mV s^{-1}. This was repeated three times. Further CV using scan rates of 0.01 mV s^{-1}, 0.05 mV s^{-1}, 0.10 mV s^{-1}, 0.20 mV s^{-1}, 0.40 mV s^{-1}, 0.50 mV s^{-1}, 0.70 mV s^{-1} and 0.80 mV s^{-1} were conducted. All CV measurements were conducted twice with a VSP Potentiostat by BioLogic. Rate capability experiments were performed by cycling three-electrode cells in a potential range of 3.0 to 4.0 V *vs.* Li|Li^+ and with different specific currents. 0.02 A g^{-1}, 0.05 A g^{-1}, 0.1 A g^{-1}, 0.2 A g^{-1}, 0.5 A g^{-1}, 1.0 A g^{-1}, 2.0 A g^{-1}, 5.0 A g^{-1} and 0.1 A g^{-1} were used for four charge and discharge cycles each. For CCC, the cells were cycled in a voltage range of 3.0 to 4.0 V with three cycles at a specific current of 0.02 A g^{-1} followed by cycling at a specific current of either 0.1 or 1.0 A g^{-1}. Three cells were prepared for rate performance tests and CCC for each electrolyte. For studies of the Li plating and stripping behaviour, different current densities were applied in symmetric Li metal||Li metal cells. Five cycles with 0.1 mA cm^{-2}, 0.2 mA cm^{-2}, 0.5 mA cm^{-2}, 1.0 mA cm^{-2}, 1.5 mA cm^{-2}, 2.0 mA cm^{-2} and 2.5 mA cm^{-2} for 1 h each and with 2 h rest step after each 5th cycle were used. Each

measurement was repeated once. A Maccor 4000 battery tester was used for the last-mentioned measurements. For EIS measurements, an OCV step of 6 h and three formation cycles with a specific current of 0.02 $A g^{-1}$ in a potential range of 3.0 to 4.0 V *vs.* $Li|Li^+$ were conducted. Before each measurement, the cells were charged for 2.5 h at 0.02 $A g^{-1}$ followed by a rest step of 6 h to reach a stable WE potential. EIS measurements of symmetric cells were conducted by cycling PTMA||Li metal cells for three cycles at 0.02 $A g^{-1}$ and one charge step limited to 2.5 h followed by an OCV step of 6 h. The cells were disassembled and two PTMA electrodes (SOC = 50 %) were reassembled into symmetric PTMA||PTMA cells without washing the electrodes. 120 µl of additional electrolyte was used for each symmetric cell. A rest step of 30 min was applied before the EIS measurement. A range of 100 kHz to 10 mHz and an amplitude of 10 mV was used. A VSP Potentiostat by BioLogic was used for all EIS measurements.

Surface Analysis of PTMA Electrodes

Cells, which were cycled for 1000 cycles at 0.1 $A g^{-1}$ and 1.0 $A g^{-1}$, were disassembled and the cycled PTMA electrode was washed with 1 ml GBL to remove residues of the conducting salt. Afterwards, the electrode was investigated *via* SEM (Carl Zeiss AURIGA) with an accelerating voltage of 3 kV.

CRediT Authorship Contribution Statement

Katharina Rudolf - Conceptualization, Investigation (lead), Writing - Original draft preparation, **Linus Voigt** - Investigation (supporting), **Simon Muench** - Resources, Writing - Review & Editing, **Lars Frankenstein** - Investigation (supporting), **Justin Landsmann** - Investigation (supporting), **Ulrich S. Schubert** - Funding Acquisition, Writing - Review & Editing, **Martin Winter** - Funding Acquisition, Supervision, Writing - Review & Editing, **Tobias Placke** - Supervision, Writing - Review & Editing, **Johannes Kasnatscheew** - Writing - Review & Editing

Acknowledgements

The authors acknowledge the German research foundation (DFG) for funding within the priority program SPP 2248 "Polymer-based Batteries". Further, the authors would like to thank Andre Bar for graphical support. Open Access funding enabled and organized by Projekt DEAL.

Conflict of Interests

The authors declare no conflict of interest.

Data Availability Statement

The data that support the findings of this study are available from the corresponding author upon reasonable request.

Keywords: Dual-ion batteries · Polymer-based cathodes · lithium salts · Fast charge · High power

[1] T. Placke, R. Kloepsch, S. Dühnen, M. Winter, *J. Solid State Electrochem.* **2017**, *21*, 1939–1964.
[2] R. Schmuch, R. Wagner, G. Hörpel, T. Placke, M. Winter, *Nat. Energy* **2018**, *3*, 267–278.
[3] T. Placke, A. Heckmann, R. Schmuch, P. Meister, K. Beltrop, M. Winter, *Joule* **2018**, *2*, 2528–2550.
[4] D. Larcher, J.-M. Tarascon, *Nat. Chem.* **2015**, *7*, 19–29.
[5] S. Muench, A. Wild, C. Friebe, B. Häupler, T. Janoschka, U. S. Schubert, *Chem. Rev.* **2016**, *116*, 9438–9484.
[6] J. E. Frerichs, L. Haneke, M. Winter, M. R. Hansen, T. Placke, *J. Power Sources Adv.* **2021**, *12*, 100075.
[7] J. M. Wrogemann, S. Künne, A. Heckmann, I. A. Rodríguez-Pérez, V. Siozios, B. Yan, J. Li, M. Winter, K. Beltrop, T. Placke, *Adv. Energy Mater.* **2020**, *10*, 1902709.
[8] a) A. Weichert, V. Göken, O. Fromm, T. Beuse, M. Winter, M. Börner, *J. Power Sources* **2022**, *551*, 232179; b) H. Chen, Z. Wu, M. Zheng, T. Liu, C. Yan, J. Lu, S. Zhang, *Mater. Today* **2022**, *52*, 364–388; c) Z. Huang, Y. Zhu, Y. Kong, Z. Wang, K. He, J. Qin, Q. Zhang, C. Su, Y. L. Zhong, H. Chen, *Adv. Funct. Mater.* **2023**, *33*; d) M. Li, H. Chen, C. Guo, S. Qian, H. Li, Z. Wu, C. Xing, P. Xue, S. Zhang, *Adv. Energy Mater.* **2023**, *13*; e) C. Chen, C.-S. Lee, Y. Tang, *Nano-Micro Lett.* **2023**, *15*, 121.
[9] a) L. Haneke, J. E. Frerichs, A. Heckmann, M. M. Lerner, T. Akbay, T. Ishihara, M. R. Hansen, M. Winter, T. Placke, *J. Electrochem. Soc.* **2020**, *167*, 140526; b) J. M. Wrogemann, et al., *Angew. Chem. Int. Ed.* **2023**, e202303111; c) B. Wei, Y. Hong, W. Tang, M. Guo, X. He, C. Tang, J. Hu, C. Fan, *Chem. Eng. J.* **2023**, *451*, 138773; d) X. He, B. Wei, W. Tang, M. Guo, J. Hu, Z. Lin, C. Fan, *Adv. Funct. Mater.* **2024**, *34*; e) Y. Li, B. Wang, *Battery Energy* **2023**, *2*; f) H. Wu, S. Luo, L. Li, H. Xiao, W. Yuan, *Battery Energy* **2023**, *2*; g) H. Wu, T. Hu, S. Chang, L. Li, W. Yuan, *ACS Appl. Mater. Interfaces* **2021**, *13*, 44254–44265.
[10] S. Muench, P. Gerlach, R. Burges, M. Strumpf, S. Hoeppener, A. Wild, A. Lex-Balducci, A. Balducci, J. C. Brendel, U. S. Schubert, *ChemSusChem* **2021**, *14*, 449–455.
[11] T. Janoschka, M. D. Hager, U. S. Schubert, *Adv. Mater.* **2012**, *24*, 6397–6409.
[12] K. Nakahara, S. Iwasa, M. Satoh, Y. Morioka, J. Iriyama, M. Suguro, E. Hasegawa, *Chem. Phys. Lett.* **2002**, *359*, 351–354.
[13] K. Nakahara, K. Oyaizu, H. Nishide, *J. Mater. Chem.* **2012**, *22*, 13669–13673.
[14] J. Kim, G. Cheruvally, J. Choi, J. Ahn, S. Lee, D. Choi, C. Song, *Solid State Ionics* **2007**, *178*, 1546–1551.
[15] A. Innocenti, I. Á. Moisés, O. Lužanin, J. Bitenc, J.-F. Gohy, S. Passerini, *ACS Appl. Mater. Interfaces* **2023**.
[16] a) J. Hu, et al., *Energy Storage Mater.* **2023**, *56*, 267–299; b) T. Zhou, W. Jin, W. Xue, B. Dai, C. Feng, X. Huang, P. Théato, Y. Li, *J. Power Sources* **2021**, *483*, 229136.
[17] J.-K. Kim, G. Cheruvally, J.-H. Ahn, Y.-G. Seo, D. S. Choi, S.-H. Lee, C. E. Song, *J. Ind. Eng. Chem.* **2008**, *14*, 371–376.
[18] a) A. D. Easley, L. M. Vukin, P. Flouda, D. L. Howard, J. L. Pena, J. L. Lutkenhaus, *Macromol.* **2020**, *53*, 7997–8008; b) P. Gerlach, R. Burges, A. Lex-Balducci, U. S. Schubert, A. Balducci, *J. Electrochem. Soc.* **2020**, *167*, 120546.
[19] P. Gerlach, A. Balducci, *Electrochim. Acta* **2021**, *377*, 138070.
[20] P. Gerlach, R. Burges, A. Lex-Balducci, U. S. Schubert, A. Balducci, *J. Power Sources* **2018**, *405*, 142–149.
[21] T. Suga, H. Konishi, H. Nishide, *Chem. Commun.* **2007**, 1730–1732.
[22] K. Nakahara, J. Iriyama, S. Iwasa, M. Suguro, M. Satoh, E. J. Cairns, *J. Power Sources* **2007**, *165*, 870–873.
[23] J.-K. Kim, J.-H. Ahn, G. Cheruvally, G. S. Chauhan, J.-W. Choi, D.-S. Kim, H.-J. Ahn, S. H. Lee, C. E. Song, *Met. Mater. Int.* **2009**, *15*, 77–82.
[24] K. Xu, *Chem. Rev.* **2004**, *104*, 4303–4417.
[25] H. Nishide, S. Iwasa, Y.-J. Pu, T. Suga, K. Nakahara, M. Satoh, *Electrochim. Acta* **2004**, *50*, 827–831.
[26] S. Wang, F. Li, A. D. Easley, J. L. Lutkenhaus, *Nat. Mater.* **2019**, *18*, 69–75.
[27] a) D. Klein-Marcuschamer, B. A. Simmons, H. W. Blanch, *Biofuels Bioprod. Biorefin.* **2011**, *5*, 562–569; b) N. V. Plechkova, K. R. Seddon, *Chem. Soc. Rev.* **2008**, *37*, 123–150.
[28] D. Belov, D.-T. Shieh, *J. Solid State Electrochem.* **2012**, *16*, 603–615.
[29] J. Kasnatscheew, R. W. Schmitz, R. Wagner, M. Winter, R. Schmitz, *J. Electrochem. Soc.* **2013**, *160*, A1369–A1374.

[30] a) K. Xu, S. Zhang, T. R. Jow, W. Xu, C. A. Angell, *Electrochem. Solid-State Lett.* **2002**, *5*, A26–A29; b) S. Shui Zhang, *Electrochem. Commun.* **2006**, *8*, 1423–1428.
[31] S. Jurng, Z. L. Brown, J. Kim, B. L. Lucht, *Energy Environ. Sci.* **2018**, *11*, 2600–2608.
[32] A. Chagnes, B. Carré, P. Willmann, R. Dedryvère, D. Gonbeau, D. Lemordant, *J. Electrochem. Soc.* **2003**, *150*, A1255–A1261.
[33] M. Ue, *J. Electrochem. Soc.* **1994**, *141*, 3336–3342.
[34] J. M. Wrogemann, et al., *Adv. Sci.* **2022**, *9*, e2201116.
[35] a) M. Ue, A. Murakami, S. Nakamura, *J. Electrochem. Soc.* **2002**, *149*, A1385–A1388; b) F. Wu, Q. Zhu, R. Chen, N. Chen, Y. Chen, L. Li, *Nano Energy* **2015**, *13*, 546–553.
[36] A. Chagnes, B. Carré, P. Willmann, D. Lemordant, *J. Power Sources* **2002**, *109*, 203–213.
[37] a) Y. Ein-Eli, S. F. McDevitt, R. Laura, *J. Electrochem. Soc.* **1998**, *145*, L1–L3; b) Y. Ein-Eli, S. R. Thomas, V. Koch, D. Aurbach, B. Markovsky, A. Schechter, *J. Electrochem. Soc.* **1996**, *143*, L273–L277.
[38] J. E. Harlow, et al., *J. Electrochem. Soc.* **2019**, *166*, A3031–A3044.
[39] A. J. Bard, L. R. Faulkner, *Electrochemical methods. Fundamentals and applications*, 2. edition ed., Wiley, New York, Weinheim, **2001**.
[40] J.-K. Kim, *J. Power Sources* **2013**, *242*, 683–686.
[41] E. Krämer, T. Schedlbauer, B. Hoffmann, L. Terborg, S. Nowak, H. J. Gores, S. Passerini, M. Winter, *J. Electrochem. Soc.* **2013**, *160*, A356–A360.
[42] P. Meister, X. Qi, R. Kloepsch, E. Krämer, B. Streipert, M. Winter, T. Placke, *ChemSusChem* **2017**, *10*, 804–814.
[43] Z. L. Brown, B. L. Lucht, *J. Electrochem. Soc.* **2019**, *166*, A5117–A5121.
[44] T. Schedlbauer, U. C. Rodehorst, C. Schreiner, H. J. Gores, M. Winter, *Electrochim. Acta* **2013**, *107*, 26–32.
[45] a) L. Stolz, G. Homann, M. Winter, J. Kasnatscheew, *Mater Adv* **2021**, *2*, 3251–3256; b) G. Homann, L. Stolz, J. Nair, I. C. Laskovic, M. Winter, J. Kasnatscheew, *Sci. Rep.* **2020**, *10*, 4390; c) S. Klein, P. Bärmann, L. Stolz, K. Borzutzki, J.-P. Schmiegel, M. Börner, M. Winter, T. Placke, J. Kasnatscheew, *ACS Appl. Mater. Interfaces* **2021**, *13*, 57241–57251.
[46] G. Homann, L. Stolz, M. Winter, J. Kasnatscheew, *iScience* **2020**, *23*, 101225.
[47] S. Klein, et al., *Adv. Energy Mater.* **2022**, *12*, 2102599.
[48] S. Klein, S. van Wickeren, S. Röser, P. Bärmann, K. Borzutzki, B. Heidrich, M. Börner, M. Winter, T. Placke, J. Kasnatscheew, *Adv. Energy Mater.* **2021**, *11*.
[49] J. E. Harlow, S. L. Glazier, J. Li, J. R. Dahn, *J. Electrochem. Soc.* **2018**, *165*, A3595–A3601.
[50] a) V. Augustyn, J. Come, M. A. Lowe, J. W. Kim, P.-L. Taberna, S. H. Tolbert, H. D. Abruña, P. Simon, B. Dunn, *Nat. Mater.* **2013**, *12*, 518–522; b) H. Lindström, S. Södergren, A. Solbrand, H. Rensmo, J. Hjelm, A. Hagfeldt, S.-E. Lindquist, *J. Phys. Chem. B* **1997**, *101*, 7717–7722.
[51] a) M. Cimenti, A. C. Co, V. I. Birss, J. M. Hill, *Fuel Cells* **2007**, *7*, 364–376; b) M. Cimenti, V. I. Birss, J. M. Hill, *Fuel Cells* **2007**, *7*, 377–391.
[52] J. Landesfeind, D. Pritzl, H. A. Gasteiger, *J. Electrochem. Soc.* **2017**, *164*, A1773–A1783.
[53] L. Stolz, M. Winter, J. Kasnatscheew, *J. Solid State Electrochem.* **2024**.
[54] a) J. Huang, *Electrochim. Acta* **2018**, *281*, 170–188; b) J. Bisquert, G. Garcia-Belmonte, F. Fabregat-Santiago, P. R. Bueno, *J. Electroanal. Chem.* **1999**, *475*, 152–163.
[55] L. Stolz, G. Homann, M. Winter, J. Kasnatscheew, *Mater. Today* **2021**, *44*, 9–14.

Manuscript received: March 22, 2024
Revised manuscript received: April 30, 2024
Accepted manuscript online: May 15, 2024
Version of record online: June 18, 2024